RSC Advances

PAPER

View Article Online
View Journal | View Issue

Check for updates

Cite this: *RSC Adv.*, 2018, **8**, 30396

Photoluminescence properties of novel $Ba_2Lu_5B_5O_{17}$:Eu^{3+} red emitting phosphors with high color purity for near-UV excited white light emitting diodes

G. Annadurai, Balaji Devakumar, Heng Guo, Bin Li, Liangling Sun and Xiaoyong Huang *

Received 31st July 2018
Accepted 23rd August 2018

DOI: 10.1039/c8ra06457a

rsc.li/rsc-advances

A series of new red-emitting $Ba_2Lu_{4.98-x}Eu_xLa_{0.02}B_5O_{17}$ ($0.1 \le x \le 1.0$) phosphors were synthesized *via* the high-temperature solid-state reaction method. The phase formation of the as-synthesized $Ba_2Lu_{4.48}Eu_{0.5}La_{0.02}B_5O_{17}$ phosphor was confirmed by powder X-ray diffraction analysis. It was found that La^{3+} doping resulted in the reduction of $LuBO_3$ impurities and thus pure phase $Ba_2Lu_5B_5O_{17}$ was realised. The morphology of $Ba_2Lu_{4.48}Eu_{0.5}La_{0.02}B_5O_{17}$ phosphors was studied by field emission scanning electron microscopy (FE-SEM). As a function of Eu^{3+} concentration the photoluminescence spectra and decay lifetimes were investigated in detail. Under excitation at 396 nm, a dominant red emission peak located at 616 nm ($^5D_0 \rightarrow {}^7F_2$) indicated that Eu^{3+} ions mainly occupied low symmetry sites with a non-inversion center in $Ba_2Lu_{4.48}Eu_{0.5}La_{0.02}B_5O_{17}$. The optimal Eu^{3+} ion concentration was found to be $x = 0.5$ and the critical distance of Eu^{3+} was determined to be 6.55 Å. In addition, the concentration quenching takes place *via* dipole–dipole interactions. The phosphors exhibited good CIE (Commission International de l'Eclairage) color coordinates ($x = 0.643$, $y = 0.356$) situated in the red region and a high color purity of 97.8%. Furthermore, the internal quantum efficiency and the thermal stability of $Ba_2Lu_{4.48}Eu_{0.5}La_{0.02}B_5O_{17}$ phosphors were also investigated systematically. The results suggest that $Ba_2Lu_{4.48}Eu_{0.5}La_{0.02}B_5O_{17}$ may be a potential red phosphor for white light-emitting diodes.

1. Introduction

The next generation light source of solid state lighting (SSL) technology would be the phosphor-converted white light-emitting diodes (pc-WLEDs) which might solve the critical issues of energy saving and reduced carbon dioxide (CO_2) emission. Compared to conventional lighting sources such as incandescent and fluorescent lamps, WLEDs have attracted great attention owing to their numerous advantages such as small volume, low power consumption, high brightness, better flexible design, reliability, long persistence and eco-friendly nature.[1–9] There exists a deficiency of red components in the commercially available WLEDs composed of blue emitting InGaN LED chips coated with a yellow $Y_3Al_5O_{12}$:Ce^{3+} phosphor.[10,11] Nevertheless, some factors that are involved in reducing the quality of white light include a low color rendering index (CRI), high correlated color temperature (CCT), thermal quenching, blue-halo effect and current dependence of chromaticity.[10,12–14] An effective solution to overcome these disadvantages would be to attain a high-quality white light by combining a near-ultraviolet (near-UV) LED chip with three primary (red, green and blue) colored phosphors.[13,15–17]

The efficiency of commercial green (ZnS:Cu^+,Al^{3+}) and blue ($BaMgAl_{10}O_{17}$:Eu^{2+}) phosphors is much higher than that of commercial red (CaS:Eu^{2+}, Y_2O_2S:Eu^{3+} and Y_2O_3:Eu^{3+}) phosphors.[15,18,19] However, the sulfide and oxysulfide based red phosphors have poor chemical stability and high toxicity, and decompose at high temperature.[18,20] The other commercial red phosphors like Eu^{2+} activated nitride compounds ($CaAlSiN_3$ and $Sr_2Si_5N_8$) have several drawbacks such as complex preparations and high cost.[18] Henceforth, the current research focus is to explore novel red phosphors that can be effectively excited by near-UV with improved stability and most importantly with enhanced efficiency.

In addition, it is also well known that Eu^{3+} ion serves as an effective activator in various inorganic host lattices, because they can give rise to bright red emission due to the 4f–4f transitions. Generally, Eu^{3+} emission originates from the transitions of $^5D_0 \rightarrow {}^7F_J$ ($J = 0$, 1, 2, 3, and 4).[21–23] Presently, many red phosphors such as rare-earth ions (Eu^{3+}) activated oxides have been investigated, including tungstates, molybdates, silicates, borates, phosphates and vanadates. Among these, a number of

Key Lab of Advanced Transducers and Intelligent Control System, Ministry of Education and Shanxi Province, College of Physics and Optoelectronics, Taiyuan University of Technology, Taiyuan 030024, P. R. China. E-mail: huangxy04@126.com

researches have been carried out on the investigation of borates, because these compounds are found to express high transmittance in the UV region, large birefringence, and nonlinear optical properties.[24,25] As a vital factor for inorganic phosphors, the host lattice must have good chemical and thermal stability.[26] Borate compounds have been explored extensively to serve as distinctive luminescent host lattices for phosphors owing to their high chemical stability, large bandgap, high optical damage threshold, high luminescence efficiency, low synthesis temperature.[27] Borate-based phosphors are found to have numerous applications in many fields such as optical data storage, flat panel display devices, lasers and nonlinear optics.[24] In recent years, various research groups have reported Eu^{3+} ions activated borate compounds such as $GdB_5O_9:Eu^{3+}$, $Sr_2ScLi(B_2O_5):Eu^{3+}$, $Sr_3Bi_2(BO_3)_4:Eu^{3+}$, $Ca_3(BO_3)_2:Eu^{3+}$.[28–31]

Recently, the efficient blue ($Ba_2Lu_5B_5O_{17}:Ce^{3+}$) and green ($Ba_2Lu_5B_5O_{17}:Ce^{3+}, Tb^{3+}$) phosphors was proposed by Xiao *et al.*[32,33] In our present work, we report a novel Eu^{3+} ion activated $Ba_2Lu_5B_5O_{17}$ red phosphors synthesized by solid-state reaction. A small amount of La^{3+} ion doped into $Ba_2Lu_5B_5O_{17}$ enabled to reduce the $LuBO_3$ impurities and thus realize pure phase of $Ba_2Lu_5B_5O_{17}$. To our knowledge, there is no reported literature available for the detailed photoluminescence properties of $Ba_2Lu_{4.98-x}Eu_xLa_{0.02}B_5O_{17}$. The luminescence properties of excitation and emission spectra and concentration quenching mechanism were investigated in detail. The decay curves have also been discussed. Further, the activation energy for the thermal quenching was determined from the temperature-dependent luminescence intensities. The obtained results suggest that the as-synthesized $Ba_2Lu_{4.48}Eu_{0.5}La_{0.02}B_5O_{17}$ would serve as a novel red emitting phosphor with potential application for WLEDs.

2. Experimental

2.1. Materials and synthesis

The $Ba_2Lu_{4.98-x}Eu_xLa_{0.02}B_5O_{17}$ (x = 0.1, 0.3, 0.5, 0.6, 0.7, 0.9, and 1.0) phosphors were prepared *via* high-temperature solid-state reaction. High purity of raw materials were $BaCO_3$ (analytical reagent; A.R.), Lu_2O_3 (99.99%), La_2O_3 (99.99%), H_3BO_3 (A.R.) and Eu_2O_3 (99.99%). The stoichiometric amounts of starting materials were thoroughly mixed in an agate mortar. Subsequently, the homogeneous mixture was pre-heated at 470 °C for 4 h. They were then reground and sintered at 1190 °C for 12 h in an air atmosphere. Finally, the as-synthesized samples were cooled down to room temperature naturally and ground again into a fine powder for further characterization.

2.2. Characterization

The phase formations of as-synthesized phosphors were analyzed by powder X-ray diffraction (XRD) measurements using Bruker D8 advance powder diffractometer. The diffraction patterns were scanned within the range of $15° \leq 2\theta \leq 65°$ operating at 40 kV and 40 mA (step size 0.02°) with CuKα radiation (λ = 1.5406 Å). The morphology and particle size of the as-synthesized samples were characterized by field-emission scanning electron microscopy (FE-SEM; MAIA3 TESCAN). The photoluminescence (PL), PL excitation (PLE) spectra as well as PL decay curves of phosphors were recorded on an Edinburgh FS5 spectrofluorometer equipped with both a continuous-wavelength and a pulsed (150 W) xenon lamp. The internal quantum efficiency (IQE) was also obtained using Edinburgh FS5 spectrofluorometer with an integrating sphere attachment. The PL spectra at different temperatures (303–483 K) were recorded using the same instrument equipped with a temperature controller.

3. Results and discussion

Phase purity of as-synthesized phosphors was analyzed using powder X-ray diffraction. Fig. 1 illustrates the XRD patterns of $Ba_2Lu_5B_5O_{17}$, $Ba_2Lu_{4.98}La_{0.02}B_5O_{17}$ and $Ba_2Lu_{4.98-x}Eu_xLa_{0.02}B_5O_{17}$ (x = 0.1, 0.5 and 1.0) phosphors. In previous studies, Xiao *et al.* reported that it was difficult to obtain pure phase of $Ba_2Lu_5B_5O_{17}$ due to the smaller ionic radius of Lu^{3+} compared to Y^{3+}.[32,33] Furthermore, in order to stabilize the crystal structure of $Ba_2Lu_5B_5O_{17}$, La_2O_3 was substituted for Lu^{3+} owing to its large ionic radius. From the XRD profiles, it can be seen that the $LuBO_3$ impurities were reduced after a small amount of La_2O_3 substituting for Lu_2O_3.[32,33] Apparently, all the diffraction peaks of as-synthesized samples are consistent with the previously reported data of $Ba_2Lu_5B_5O_{17}$.[32,33] The crystal structure and the cation coordination environments were investigated by Xiao *et al.*[32,33] In addition, the previously reported results reveal the orthorhombic structure of $Ba_2Lu_5B_5O_{17}$ with space group *Pbcn*(60); cell parameters a = 17.2144 Å, b = 6.5990 Å, c = 12.9587 Å; and cell volume (V) = 1472.09 Å^3.[33]

Fig. 2(a) demonstrates the FE-SEM micrograph of $Ba_2Lu_{4.48}Eu_{0.5}La_{0.02}B_5O_{17}$ phosphors prepared by solid state reaction method. In general, the synthesized samples by high temperature solid state reaction exhibit some degree of particle

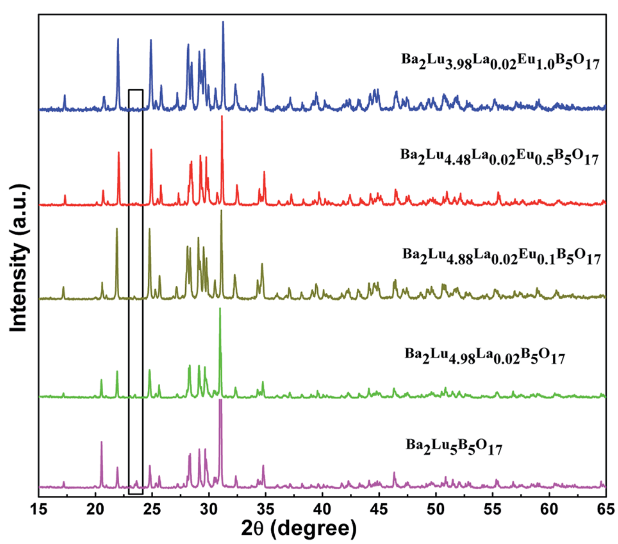

Fig. 1 XRD profiles of the $Ba_2Lu_5B_5O_{17}$, $Ba_2Lu_{4.98}La_{0.02}B_5O_{17}$ and $Ba_2Lu_{4.98-x}Eu_xLa_{0.02}B_5O_{17}$ (x = 0.1, 0.5 and 1.0) phosphors.

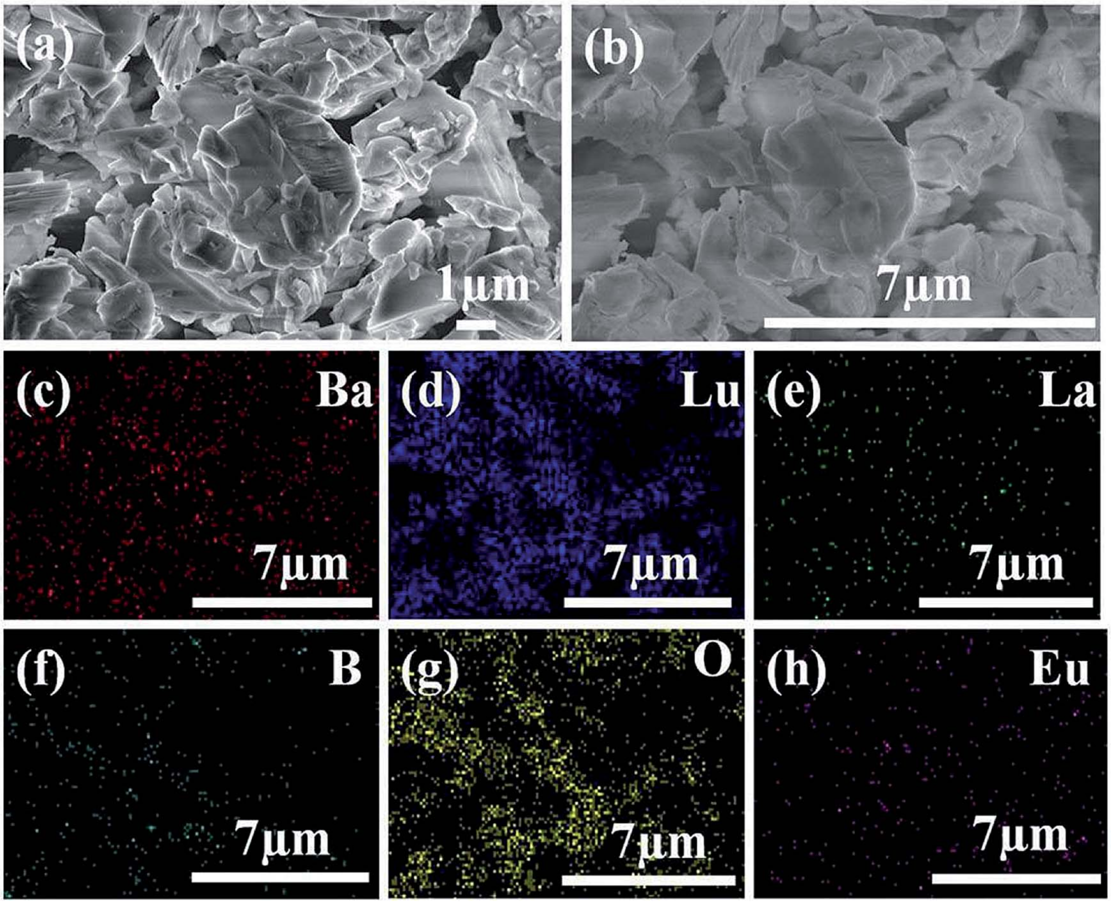

Fig. 2 (a) SEM micrograph of $Ba_2Lu_{4.48}Eu_{0.5}La_{0.02}B_5O_{17}$ phosphors. (b–h) Elemental mapping profiles of $Ba_2Lu_{4.48}Eu_{0.5}La_{0.02}B_5O_{17}$ phosphors.

agglomeration with different size distribution.[34] As can be seen from the Fig. 2(a), the as-obtained micrograph shows that the shape of the sample consists of an irregular morphology, which was ascribed to the fundamental characteristics of high temperature solid state reaction method.[35,36] The particles are agglomerated due to the sustained sintering time and intermediate grindings. The above results clearly suggest that the $Ba_2Lu_{4.48}Eu_{0.5}La_{0.02}B_5O_{17}$ phosphors could be useful for potential application in WLEDs. To confirm the homogeneity of elements in the compounds, we carried out elemental mapping. The elemental area profiles with different elements in various colors were shown in Fig. 2(b–h). The elemental mapping results of $Ba_2Lu_{4.48}Eu_{0.5}La_{0.02}B_5O_{17}$ phosphors disclosed that Ba, Lu, La, B, O and Eu elements were homogeneously distributed throughout the entire particles.

Fig. 3(a) shows the PLE and PL spectra of $Ba_2Lu_{4.48}Eu_{0.5}La_{0.02}B_5O_{17}$ phosphors at room temperature. It can be easily seen that the PLE spectrum monitored at 616 nm comprised of a broad band ranging from ~200 to 300 nm and a series of sharp peaks located in the range of ~300–550 nm. The broad band centered at 282 nm can be assigned to the charge transfer band (CTB) of $O^{2-} \rightarrow Eu^{3+}$.[15,37] The electron transfer from the $2p^6$ orbital of O^{2-} ions to the 4f orbital of Eu^{3+} ions.[38,39] The sharp excitation peak belonged to the intra-configurational 4f–4f electronic transitions of Eu^{3+} ions, in which the peaks situated at 321, 364, 382, 396, 411, 467, 524 nm correspond to the transitions from $^7F_0$ to $^5H_6$, $^5D_4$, $^5L_7$, $^5L_6$, $^5D_3$, $^5D_2$, and $^5D_1$ levels, respectively.[15,40–42] The dominant peak centered at 396 nm suggests that the phosphor can be efficiently excited by near-UV LED chip.[15]

Fig. 3(a) depicts the PL spectrum of $Ba_2Lu_{4.48}Eu_{0.5}La_{0.02}B_5O_{17}$ phosphors ($\lambda_{ex} = 396$ nm). A series of sharp peaks situated at 574, 588, 616, 655 and 707 nm correspond to the transitions from the $^5D_0$ excited state to the ^7F_J ($J = 0, 1, 2, 3$ and 4) ground states of Eu^{3+} ions.[15,40] Generally, when the Eu^{3+} ions are situated at the crystallographic sites with inversion symmetry, the magnetic dipole (MD) $^5D_0 \rightarrow {}^7F_1$ transition would be dominant; while Eu^{3+} ions occupy in a site without inversion symmetry, the electric dipole (ED) $^5D_0 \rightarrow {}^7F_2$ transition will be dominant.[43] From this spectrum, the PL intensity of (ED) $^5D_0 \rightarrow {}^7F_2$ transition at around 616 nm was stronger than that of the (MD) $^5D_0 \rightarrow {}^7F_1$ transition at around 588 nm. The above result suggested that the local symmetry of Eu^{3+} site belonged to the non-centrosymmetric site in $Ba_2Lu_{4.48}Eu_{0.5}La_{0.02}B_5O_{17}$ host lattice with beneficial color purity.[44]

The PL spectra of $Ba_2Lu_{4.98-x}Eu_xLa_{0.02}B_5O_{17}$ ($x = 0.1, 0.3, 0.5, 0.6, 0.7, 0.9$ and 1.0) phosphors with different Eu^{3+} concentration under 396 nm excitation were shown in Fig. 3(b). All the PL spectra profiles and peak positions were very similar except for their PL intensity. The dependence of Eu^{3+} concentration on PL

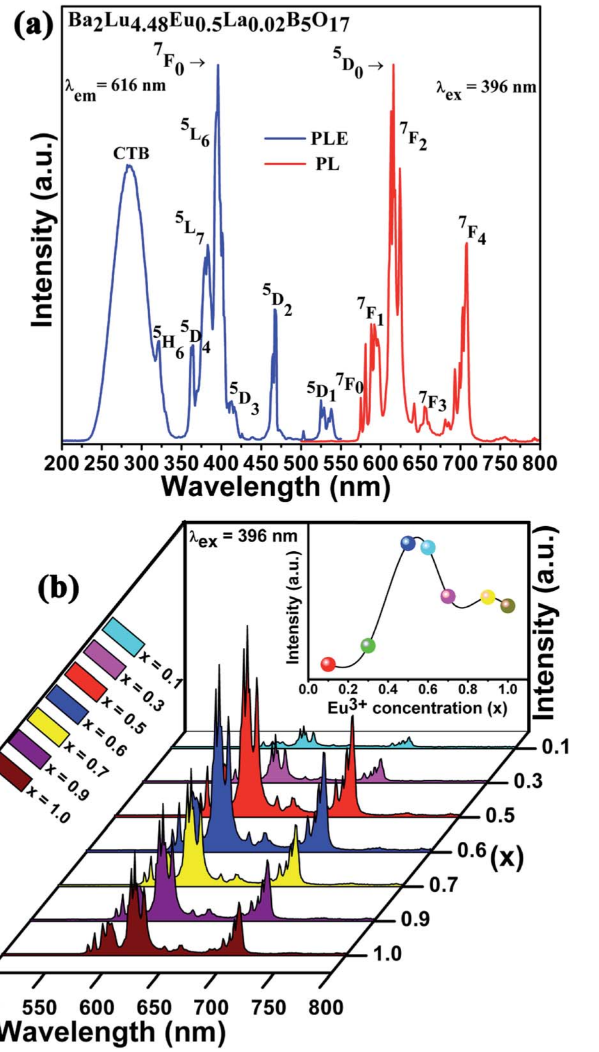

Fig. 3 (a) PLE (λ_{em} = 616 nm) and PL (λ_{ex} = 396 nm) spectra of $Ba_2Lu_{4.48}Eu_{0.5}La_{0.02}B_5O_{17}$; (b) PL spectra for $Ba_2Lu_{4.98-x}Eu_xLa_{0.02}B_5O_{17}$ (x = 0.1, 0.3, 0.5, 0.6, 0.7, 0.9 and 1.0) phosphors. Inset shows the PL intensity as a function of Eu^{3+}concentration.

intensity of $^5D_0 \rightarrow {}^7F_2$ (616 nm) transition was shown in the inset of Fig. 3(b). It can be clearly observed that the PL intensity enhanced with increasing the Eu^{3+} concentration until it reached a maximum at $x = 0.5$. Herein, the optimum concentration of Eu^{3+} was determined to be $x = 0.5$ in $Ba_2Lu_{4.98-x}Eu_xLa_{0.02}B_5O_{17}$ host. Beyond the optimum concentration, the PL intensity dramatically decreased due to the concentration quenching effect.

The concentration quenching mechanism is often attributed to energy migration between Eu^{3+} ions. In concentration quenching phenomenon, the critical distance R_c among activator is a significant parameter. When R_c is less than 5 Å, the concentration quenching is dealt to be an exchange interaction. In other cases, the R_c value is greater than 5 Å, electric multipolar interaction will be the dominant mechanism for the concentration quenching. The value of R_c can be estimated *via* the following equation proposed by Blasse:[45]

$$R_c \approx 2\left(\frac{3V}{4\pi x_c N}\right)^{1/3} \quad (1)$$

herein, V stands for the volume of the unit cell, x_c is the critical concentration of Eu^{3+} ions, and N indicates the number of host cations in the unit cell. For $Ba_2Lu_{4.98-x}Eu_xLa_{0.02}B_5O_{17}$ phosphors, $x_c = 0.5$ and the previously reported parameters of V and N were 1472.09 Å^3 and 20, respectively.[33] Therefore, R_c was determined to be about 6.55 Å. In the present case, R_c value was found to be greater than 5 Å, and it can be reasonable to resolve that the exchange interaction was not responsible in $Ba_2Lu_{4.98-x}Eu_xLa_{0.02}B_5O_{17}$ phosphors. Hence, the energy transfer between Eu^{3+} ions mainly took place *via* multipolar interactions. According to the Dexter's theory, the multipolar interaction can be explained by the following equation:[46]

$$\frac{I}{x} = k\left[1 + \beta(x)^{\theta/3}\right]^{-1} \quad (2)$$

where x is the concentration of Eu^{3+} ions, I/x represents the emission intensity per activator concentration, k and β are constants for the given host at the same excitation conditions; θ stands for the electric multipolar interaction, when the value of θ is 3, 6, 8 or 10 corresponding to the exchange interaction, dipole–dipole (d–d), dipole–quadrupole (d–q) or quadrupole–quadrupole (q–q) interactions, respectively.[47] The eqn (2) can be simplified by assuming $\beta(x) \gg 1$:[48,49]

$$\log\left(\frac{I}{x}\right) = K' - \frac{\theta}{3}\log(x) \quad (3)$$

where $K' = \log k - \log \beta$. Fig. 4 shows the dependence of $\log(I/x)$ on $\log(x)$. As can be seen from this figure, the fitting result was linear and the slope of the straight line was −1.931. Therefore, the value of θ can be calculated as ∼5.79, which is mostly close to 6. This result proposed that the d–d interaction was mainly responsible for the energy transfer between Eu^{3+} ions in $Ba_2Lu_{4.98-x}Eu_xLa_{0.02}B_5O_{17}$ phosphors.

The integrated PL intensity ratio of $R = I(^5D_0 \rightarrow {}^7F_2)/I(^5D_0 \rightarrow {}^7F_1)$ transitions, also known as

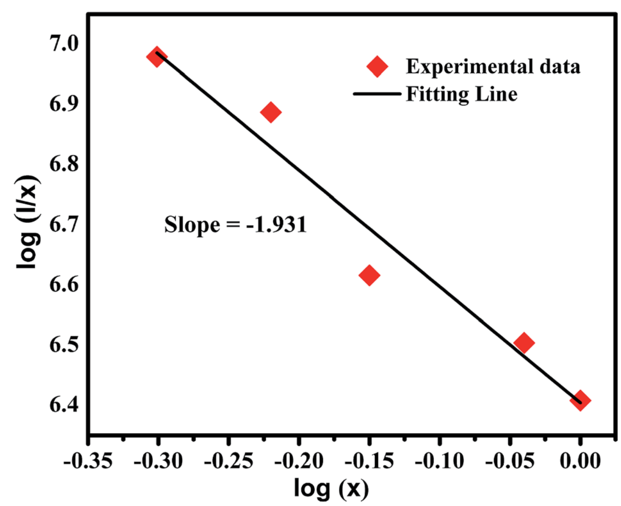

Fig. 4 The relationship of $\log(I/x)$ *versus* $\log(x)$ for $Ba_2Lu_{4.98-x}Eu_xLa_{0.02}B_5O_{17}$ phosphors.

asymmetry ratio can be used as an index to assess the site symmetry around the Eu^{3+} ions.[40,50–52] The (ED) $^5D_0 \rightarrow {}^7F_2$ transition is a hypersensitive transition as this type of transition is really sensitive to the local environment, while the (MD) $^5D_0 \rightarrow {}^7F_1$ transition is insensitive to the local environment at Eu^{3+} site.[53,54] The calculated R value for $Ba_2Lu_{4.48}Eu_{0.5}La_{0.02}B_5O_{17}$ phosphor was determined to be 2.88. The results distinctly suggest the lack of an inversion center, and thus the Eu^{3+} ion is favorable to achieve a bright red emission with high color purity.[37,55]

The PL decay curves of $Ba_2Lu_{4.98-x}Eu_xLa_{0.02}B_5O_{17}$ (x = 0.1, 0.3, 0.5, 0.6, 0.7, 0.9 and 1.0) phosphors monitored at 616 nm under excitation at 396 nm were shown in Fig. 5. All the decay curves were almost overlapping with each other. The corresponding PL decay curves can be well fitted with single exponential function by the following equation:[56]

$$I(t) = I_0 + A\exp(-t/\tau) \tag{4}$$

where $I(t)$ and I_0 are the luminescence intensities at time t and t = 0, A is a constant, and τ is the decay lifetime. From the fitted results, the effective decay lifetimes for $^5D_0 \rightarrow {}^7F_2$ transition of $Ba_2Lu_{4.98-x}Eu_xLa_{0.02}B_5O_{17}$ (x = 0.1, 0.3, 0.5, 0.6, 0.7, 0.9 and 1.0) phosphors were determined to be 1.325, 1.372, 1.409, 1.455, 1.524, 1.655 and 1.733 ms, respectively. The above results indicated that the PL lifetime values reasonably increased with increasing Eu^{3+} concentration in the structure, which can be attributed to energy migration between Eu^{3+} ions.[57–62] The fluorescence lifetime of $Ba_2Lu_{4.98-x}Eu_xLa_{0.02}B_5O_{17}$ (x = 0.1, 0.3, 0.5, 0.6, 0.7, 0.9 and 1.0) phosphor is short enough for potential application in near-UV excited WLEDs applications.

Fig. 6 depicts the CIE chromaticity diagram of optimized $Ba_2Lu_{4.48}Eu_{0.5}La_{0.02}B_5O_{17}$ phosphors under excitation at 396 nm. The corresponding CIE chromaticity coordinates were found as (0.643, 0.356), and it is located in the red region. Furthermore, the CIE chromaticity coordinates of $Ba_2Lu_{4.48}Eu_{0.5}La_{0.02}B_5O_{17}$ phosphors were nearly close to the National

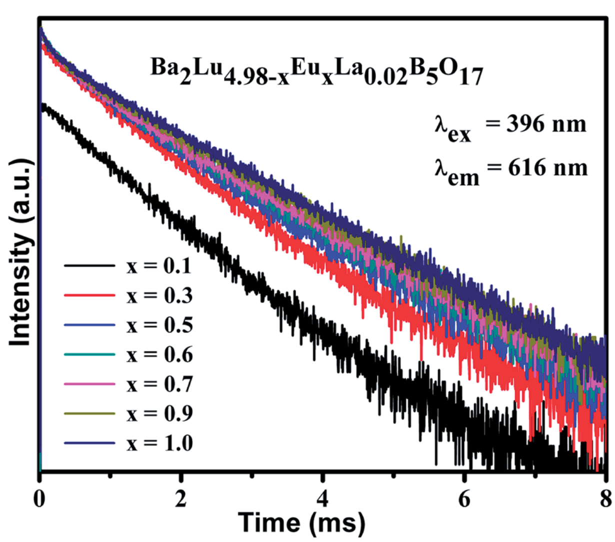

Fig. 5 PL decay curves of $Ba_2Lu_{4.98-x}Eu_xLa_{0.02}B_5O_{17}$ (x = 0.1, 0.3, 0.5, 0.6, 0.7, 0.9 and 1.0) under excited at 396 nm and monitored at 616 nm.

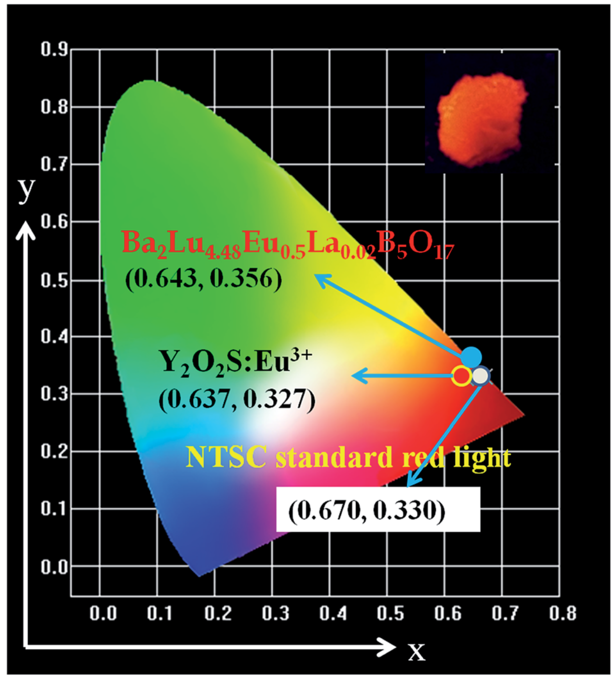

Fig. 6 CIE chromaticity diagram for $Ba_2Lu_{4.48}Eu_{0.5}La_{0.02}B_5O_{17}$ red phosphors. Inset shows the digital photograph of optimal $Ba_2Lu_{4.48}Eu_{0.5}La_{0.02}B_5O_{17}$ phosphors under 365 nm UV lamp.

Television Standard Committee (NTSC) system [CIE: (0.670, 0.330)] with superior characteristics as compared to those required for commercial $Y_2O_2S:Eu^{3+}$ red phosphors [CIE: (0.637, 0.327)].[56] The inset of Fig. 6 shows the digital photograph of $Ba_2Lu_{4.48}Eu_{0.5}La_{0.02}B_5O_{17}$ sample under 365 nm UV lamp. The color purity of as-synthesized $Ba_2Lu_{4.48}Eu_{0.5}La_{0.02}B_5O_{17}$ phosphors is an essential factor for WLEDs application. Therefore the color purity can be calculated through the following expression:[63]

$$\text{Color purity} = \frac{\sqrt{(x - x_i)^2 + (y - y_i)^2}}{\sqrt{(x_d - x_i)^2 + (y_d - y_i)^2}} \times 100\% \tag{5}$$

here, (x,y) stands for the CIE coordinates of $Ba_2Lu_{4.48}Eu_{0.5}La_{0.02}B_5O_{17}$ phosphors, (x_i,y_i) denotes the color coordinates of white illumination and (x_d,y_d) represents the coordinates of dominant wavelength, respectively. In the present work, the coordinates were evaluated to be (x = 0.643, y = 0.356), (x_i = 0.310, y_i = 0.316) and (x_d = 0.651, y_d = 0.353). According to the above equation, the color purity of $Ba_2Lu_{4.48}Eu_{0.5}La_{0.02}B_5O_{17}$ red phosphors was calculated to be 97.8%.

These results suggested that the $Ba_2Lu_{4.48}Eu_{0.5}La_{0.02}B_5O_{17}$ phosphors demonstrated good CIE chromaticity coordinates with high color purity. Additionally, the IQE of phosphors are a vital parameter for their potential application in near-UV excited WLEDs application. Hence, the IQE value for $Ba_2Lu_{4.48}Eu_{0.5}La_{0.02}B_5O_{17}$ phosphors under 396 nm excitation was determined as 27.1%, which is not highly sufficient. To achieve better performance of $Ba_2Lu_{4.48}Eu_{0.5}La_{0.02}B_5O_{17}$ phosphor, the obtained IQE value could further be enhanced by suitable

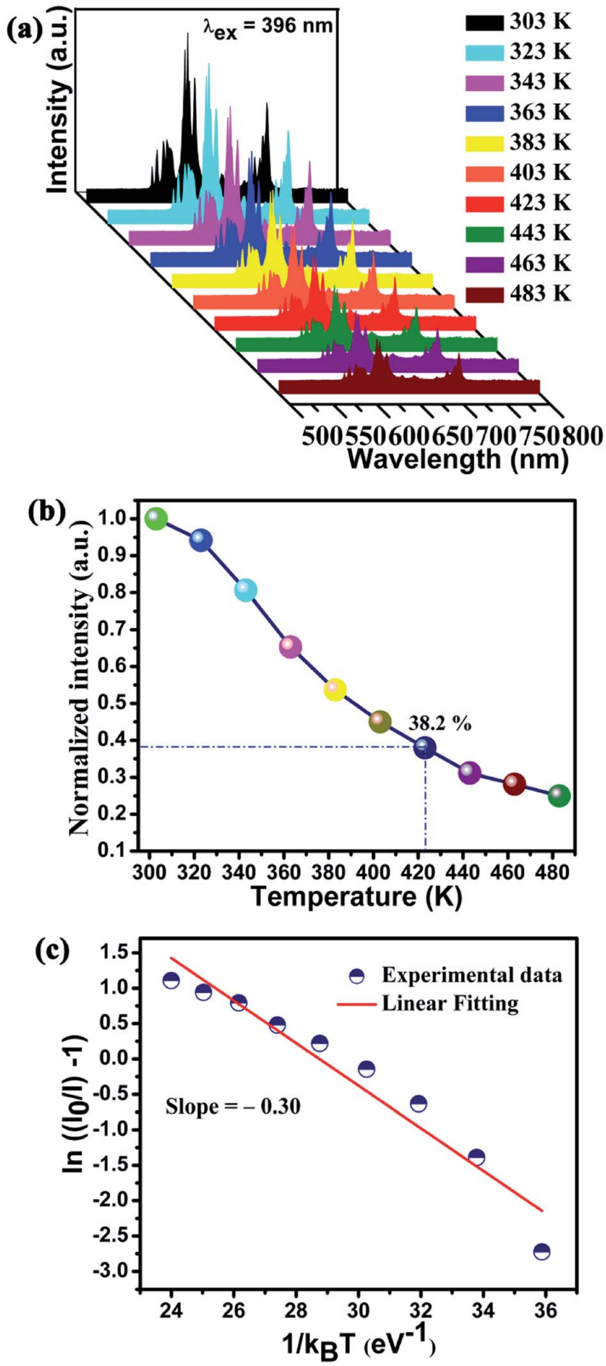

Fig. 7 (a) PL spectra of $Ba_2Lu_{4.48}Eu_{0.5}La_{0.02}B_5O_{17}$ phosphors (λ_{ex} = 396 nm) with different temperature; (b) the normalized PL intensities as a function of the temperature; (c) relationship of $\ln[(I_0/I) - 1]$ *versus* $1/k_BT$ for $Ba_2Lu_{4.48}Eu_{0.5}La_{0.02}B_5O_{17}$ phosphors.

experimental conditions, controlling the particle size, size distribution, morphology and optimization of the chemical compositions.[35,64,65]

In the action of high power WLEDs application, thermal stability of phosphor is one of the important factors. Fig. 7(a) shows the temperature dependent PL spectra of $Ba_2Lu_{4.48}Eu_{0.5}La_{0.02}B_5O_{17}$ phosphors from 303 to 483 K under excitation at 396 nm. As seen in Fig. 7(b), the normalized PL intensities of $^5D_0 \rightarrow {}^7F_2$ transition gradually decreased as the temperature increased from 303 to 483 K. The thermal quenching due to the non-radiative transition from the excited luminescence center was thermally activated by the crossing point between the excited and ground states.[40,66] The PL spectra profile slightly changed due to a decrease in the peak intensities as the temperature was raised above 403 K. It can be noted that the normalized PL intensities at 423 K still remained 38.2% of their initial intensities at 303 K. This implied that the thermal stability of $Ba_2Lu_{4.48}Eu_{0.5}La_{0.02}B_5O_{17}$ phosphor further needs to be enhanced. In order to further investigate the relationship between PL intensity and the temperature, the activation energy (ΔE_a) for thermal quenching can be described *via* the Arrhenius equation as follows:[67,68]

$$I(T) = \frac{I_o}{1 + A\exp\left(-\frac{\Delta E_a}{k_B T}\right)} \tag{6}$$

where I_o is the initial PL intensity and $I(T)$ represents the PL intensity at various temperature, k_B is the Boltzmann constant (8.629×10^{-5} eV K^{-1}) and A is a constant. Furthermore, the eqn (6) can be rearranged as the following equation:[66,69,70]

$$\ln\left[\left(\frac{I_0}{I}\right) - 1\right] = -\frac{\Delta E_a}{k_B T} + \ln c \tag{7}$$

Fig. 7(c) depicts the relationship of $\ln[(I_0/I) - 1]$ *versus* $1/k_BT$. From the slope of linear fitting, the value of ΔE_a was deduced to be ~0.30 eV for $Ba_2Lu_{4.48}Eu_{0.5}La_{0.02}B_5O_{17}$ phosphors. These results suggest necessity to enhance the PL intensity of as-synthesized phosphors for improved thermal stability which could be obtain with the optimization of experimental conditions and material compositions.[71]

4. Conclusions

In summary, the $Ba_2Lu_{4.98-x}Eu_xLa_{0.02}B_5O_{17}$ ($0.1 \le x \le 1.0$) red emitting phosphors were successfully synthesized by a traditional solid-state reaction method. The $Ba_2Lu_{4.48}Eu_{0.5}La_{0.02}B_5O_{17}$ phosphors can be effectively excited at 396 nm, which matched well with the near-UV chip. Under the excitation at 396 nm, the PL spectrum showed an intense red emission situated at 616 nm, which was certified to the Eu^{3+} ions occupied at low symmetry sites with non-inversion center. The optimum concentration of Eu^{3+} for $Ba_2Lu_{4.98-x}Eu_xLa_{0.02}B_5O_{17}$ phosphors was determined as $x = 0.5$. Also the concentration quenching took place *via* the dipole–dipole interaction. The decay lifetime of $Ba_2Lu_{4.48}Eu_{0.5}La_{0.02}B_5O_{17}$ phosphor was calculated to be 1.409 ms. As a result, the $Ba_2Lu_{4.48}Eu_{0.5}La_{0.02}B_5O_{17}$ phosphor exhibited significant red emission intensity, excellent color purity (97.8%), good color coordinates (0.643, 0.356) and the IQE of 27.1%. In addition, the activation energy for the thermal quenching (ΔE_a) was calculated to be 0.30 eV. The obtained results indicate that the $Ba_2Lu_{4.48}Eu_{0.5}La_{0.02}B_5O_{17}$ red emitting phosphors may be considered as a potential candidate for WLEDs.

Conflicts of interest

There are no conflicts to declare.

Acknowledgements

This research work was supported by the National Natural Science Foundation of China (No. 51502190), the Program for the Outstanding Innovative Teams of Higher Learning Institutions of Shanxi, and the Open Fund of the State Key Laboratory of Luminescent Materials and Devices (South China University of Technology, No. 2017-skllmd-01).

References

1 L. Zhao, F. Fan, X. Chen, Y. Wang, Y. Li and B. Deng, *J. Mater. Sci.: Mater. Electron.*, 2018, **29**, 5975–5981.
2 G. Feng, W. Jiang, J. Liu, C. Li and Q. Zhang, *Luminescence*, 2018, **33**, 455–460.
3 P. Du, X. Huang and J. S. Yu, *Chem. Eng. J.*, 2018, **337**, 91–100.
4 X. Huang and H. Guo, *RSC Adv.*, 2018, **8**, 17132–17138.
5 X. Huang, B. Li and H. Guo, *J. Alloys Compd.*, 2017, **695**, 2773–2780.
6 X. Huang and H. Guo, *Dyes Pigm.*, 2018, **152**, 36–42.
7 X. Huang, *J. Alloys Compd.*, 2017, **690**, 356–359.
8 P. Du, L. Luo, X. Huang and J. S. Yu, *J. Colloid Interface Sci.*, 2018, **514**, 172–181.
9 P. Du, X. Huang and J. S. Yu, *Inorg. Chem. Front.*, 2017, **4**, 1987–1995.
10 J. S. Kim, P. E. Jeon, Y. H. Park, J. C. Choi and H. L. Park, *J. Electrochem. Soc.*, 2005, **152**, H29–H32.
11 X. Huang, *Nat. Photonics*, 2014, **8**, 748–749.
12 G. Zhu, Y. Wang, Z. Ci, B. Liu, Y. Shi and S. Xin, *J. Electrochem. Soc.*, 2011, **158**, J236–J242.
13 M. Xia, Z. Ju, H. Yang, Z. Wang, X. Gao, F. Pan and W. Liu, *J. Alloys Compd.*, 2018, **739**, 439–446.
14 B. Li, X. Huang, H. Guo and Y. Zeng, *Dyes Pigm.*, 2018, **150**, 67–72.
15 J. Lu, Z. Mu, D. Zhu, Q. Wang and F. Wu, *J. Lumin.*, 2018, **196**, 50–56.
16 X. Huang, B. Li, H. Guo and D. Chen, *Dyes Pigm.*, 2017, **143**, 86–94.
17 S. H. Lee, Y. Cha, H. Kim, S. Lee and J. S. Yu, *RSC Adv.*, 2018, **8**, 11207–11215.
18 T. Hasegawa, S. W. Kim, T. Ueda, T. Ishigaki, K. Uematsu, H. Takaba, K. Toda and M. Sato, *J. Mater. Chem. C*, 2017, **5**, 9472–9478.
19 H. Y. Jiao and Y. Wang, *Phys. B*, 2012, **407**, 2729–2733.
20 L. L. Ying, S. S. Zheng, J. H. Zheng, L. H. Cai and C. Chen, *Adv. Mater. Res.*, 2014, **1003**, 7–10.
21 L. L. Devi and C. Jayasankar, *Ceram. Int.*, 2018, **44**, 14063–14069.
22 X. Huang, H. Guo and B. Li, *J. Alloys Compd.*, 2017, **720**, 29–38.
23 X. Huang, S. Wang, B. Li, Q. Sun and H. Guo, *Opt. Lett.*, 2018, **43**, 1307–1310.
24 A. A. Reddy, S. Das, S. Ahmad, S. S. Babu, J. M. Ferreira and G. V. Prakash, *RSC Adv.*, 2012, **2**, 8768–8776.
25 M. He, G. Huang, H. Tao and Z. Zhang, *Phys. B*, 2012, **407**, 2725–2728.
26 X. Zhang, Y. Chen, S. Zeng, L. Zhou, J. Shi and M. Gong, *Ceram. Int.*, 2014, **40**, 14537–14541.
27 F. Xiong, J. Luo, H. Lin, X. Meng, Y. Wang, H. Shen and W. Zhu, *Optik*, 2018, **156**, 31–38.
28 A. Kruopyte, R. Giraitis, R. Juskenas, D. Enseling, T. Jüstel and A. Katelnikovas, *J. Lumin.*, 2017, **192**, 520–526.
29 B. Bondzior and P. Dereń, *New J. Chem.*, 2017, **41**, 7662–7666.
30 A. Shablinskii, R. Bubnova, I. Kolesnikov, M. Krzhizhanovskaya, A. Povolotskiy, V. Ugolkov and S. Filatov, *Solid State Sci.*, 2017, **70**, 93–100.
31 H. Huang, X. Feng, T. Chen, Y. Xiong and F. Zhang, *Luminescence*, 2018, **33**, 692–697.
32 Y. Xiao, Z. Hao, L. Zhang, H. Wu, G.-H. Pan, X. Zhang and J. Zhang, *Dyes Pigm.*, 2018, **154**, 121–127.
33 Y. Xiao, Z. Hao, L. Zhang, X. Zhang, G.-H. Pan, H. Wu, H. Wu, Y. Luo and J. Zhang, *J. Mater. Chem. C*, 2018, **6**, 5984–5991.
34 J. Zhang, M. Chen and Y. Gao, *Displays*, 2017, **49**, 35–39.
35 Y. Wang, X. Liu, P. Niu, L. Jing and W. Zhao, *J. Lumin.*, 2017, **184**, 1–6.
36 H. Guo and X. Huang, *J. Alloys Compd.*, 2018, **764**, 809–814.
37 J. Qiao, L. Wang, Y. Liu, P. Huang, Q. Shi and Y. Tian, *J. Alloys Compd.*, 2016, **686**, 601–607.
38 B. G. Vats, S. K. Gupta, M. Keskar, R. Phatak, S. Mukherjee and S. Kannan, *New J. Chem.*, 2016, **40**, 1799–1806.
39 W. Zhang, X. Yin, Y. Liu, N. Zhang, G. Zhao, J. Hou and Y. Fang, *J. Mater. Sci.: Mater. Electron.*, 2016, **27**, 5357–5361.
40 J. Chen, W. Zhao, J. Wang and N. Wang, *J. Mater. Sci.: Mater. Electron.*, 2016, **27**, 237–244.
41 J. Liang, P. Du, H. Guo, L. Sun, B. Li and X. Huang, *Dyes Pigm.*, 2018, **157**, 40–46.
42 L. Sun, H. Guo, J. Liang, B. Li and X. Huang, *J. Lumin.*, 2018, **202**, 403–408.
43 X. Huang, B. Li and H. Guo, *Ceram. Int.*, 2017, **43**, 10566–10571.
44 K. Singh and S. Vaidyanathan, *ChemistrySelect*, 2016, **1**, 5448–5462.
45 G. Blasse, *J. Solid State Chem.*, 1986, **62**, 207–211.
46 D. L. Dexter, *J. Chem. Phys.*, 1953, **21**, 836–850.
47 L. Van Uitert, *J. Electrochem. Soc.*, 1967, **114**, 1048–1053.
48 S. Xin, Y. Wang, Z. Wang, F. Zhang, Y. Wen and G. Zhu, *ECS Solid State Lett.*, 2011, **14**, H438–H441.
49 D. Dexter and J. H. Schulman, *J. Chem. Phys.*, 1954, **22**, 1063–1070.
50 J. Zhu, Z. Xia, Y. Zhang, M. S. Molokeev and Q. Liu, *Dalton Trans.*, 2015, **44**, 18536–18543.
51 Z.-w. Zhang, L. Liu, R. Liu, X.-y. Zhang, X.-g. Peng, C.-h. Wang and D.-j. Wang, *Mater. Lett.*, 2016, **167**, 250–253.
52 J. Llanos, D. Espinoza and R. Castillo, *RSC Adv.*, 2017, **7**, 14974–14980.
53 J. Liao, B. Qiu, H.-R. Wen, Y. Li, R. Hong and H. You, *J. Mater. Sci.*, 2011, **46**, 1184–1189.
54 P. Du, Y. Guo, S. H. Lee and J. S. Yu, *RSC Adv.*, 2017, **7**, 3170–3178.

55 H. Guo, H. Zhang, R. Wei, M. Zheng and L. Zhang, *Opt. Express*, 2011, **19**, A201–A206.
56 H. Guo, X. Huang and Y. Zeng, *J. Alloys Compd.*, 2018, **741**, 300–306.
57 Y. Zhang, W. Gong and G. Ning, *New J. Chem.*, 2016, **40**, 10136–10143.
58 A. Fu, A. Guan, F. Gao, X. Zhang, L. Zhou, Y. Meng and H. Pan, *Opt. Laser Technol.*, 2017, **96**, 43–49.
59 J. Grigorjevaite and A. Katelnikovas, *ACS Appl. Mater. Interfaces*, 2016, **8**, 31772–31782.
60 L. Mengting and J. Baoxiang, *J. Rare Earths*, 2015, **33**, 231–238.
61 G. Annadurai, B. Devakumar, H. Guo, R. Vijayakumar, B. Li, L. Sun, X. Huang, K. Wang and X. W. Sun, *RSC Adv.*, 2018, **8**, 23323–23331.
62 R. Vijayakumar, B. Devakumar, G. Annadurai, H. Guo and X. Huang, *Opt. Mater.*, 2018, **84**, 312–317.
63 Y. Wu, K. Qiu, Q. Tang, W. Zhang and J. Wang, *Ceram. Int.*, 2018, **44**, 8190–8195.
64 X. Zhang, Z.-C. Wu, Y. Li, J. Xu and L. Tian, *Dyes Pigm.*, 2017, **144**, 94–101.
65 X. Chen, Q. Wang, F. Lv, P. K. Chu and Y. Zhang, *RSC Adv.*, 2016, **6**, 11211–11217.
66 K. Li, S. Liang, M. Shang, H. Lian and J. Lin, *Inorg. Chem.*, 2016, **55**, 7593–7604.
67 M. Zhou, H. Ming, J. Peng, Y. Qiang and X. Ye, *ECS J. Solid State Sci. Technol.*, 2017, **6**, R175–R182.
68 J. Zhong, D. Chen, H. Xu, W. Zhao, J. Sun and Z. Ji, *J. Alloys Compd.*, 2017, **695**, 311–318.
69 W. Guo, Y. Tian, P. Huang, L. Wang and Q. Shi, *Ceram. Int.*, 2016, **42**, 5427–5432.
70 Q. Liu, X. Li, B. Zhang, L. Wang, Q. Zhang and L. Zhang, *Ceram. Int.*, 2016, **42**, 15294–15300.
71 X. Wang, Z. Zhao, Q. Wu, Y. Li and Y. Wang, *Inorg. Chem.*, 2016, **55**, 11072–11077.